

R 12

**INVESTIGATION OF THE AEROELASTIC STABILITY OF THE
AFW WIND-TUNNEL MODEL USING CAP-TSD**

WALTER A. SILVA AND ROBERT M. BENNETT

(NASA-TM-104142) INVESTIGATION OF THE
AEROELASTIC STABILITY OF THE AFW WIND-TUNNEL
MODEL USING CAP-TSD (NASA) 12 p CSCL 01A

N92-11977

Unclas
G3/02 0051758

SEPTEMBER 1991



National Aeronautics and
Space Administration

Langley Research Center
Hampton, Virginia 23665

INVESTIGATION OF THE AEROELASTIC STABILITY OF THE AFW WIND-TUNNEL MODEL USING CAP-TSD

Walter A. Silva and Robert M. Bennett
Unsteady Aerodynamics Branch
NASA Langley Research Center
Hampton, VA 23665-5225

1. SUMMARY

The CAP-TSD (Computational Aeroelasticity Program - Transonic Small Disturbance) code, developed at the NASA - Langley Research Center, is applied to the Active Flexible Wing (AFW) wind-tunnel model for prediction of the model's transonic aeroelastic behavior. A semi-span computational model is used for evaluation of symmetric motions and a full-span model is used for evaluation of antisymmetric motions. Static aeroelastic solutions using CAP-TSD are computed. Dynamic (flutter) analyses are then performed as perturbations about the static aeroelastic deformations and presented as flutter boundaries in terms of Mach number and dynamic pressure. Flutter boundaries that take into account modal refinements, vorticity and entropy corrections, antisymmetric motions and sensitivity to the modeling of the wing tip ballast stores are also presented and compared with experimental flutter results.

2. INTRODUCTION

An understanding of the aeroelastic behavior of flight vehicles in the transonic regime is of great importance for flight safety. For example, it is well known that aircraft flying into or through the transonic regime may encounter a region of reduced flutter speed known as the transonic flutter dip. Valuable insight into the nature of this transonic flutter dip phenomena is provided by Isogai¹ for a typical, two-dimensional streamwise section of an aft-swept wing, while comparison of aerodynamic theory with the experiments reported by Davis and Malcolm² reveals the limitations of linear theory when applied in the transonic regime. Linear aerodynamics, although highly successful in the subsonic and supersonic regimes, cannot normally be used to accurately predict transonic aeroelastic behavior. Transonic flow equations capable of modelling flow nonlinearities (shocks, boundary layer, separation and vorticity) and boundary condition nonlinearities (airfoil thickness and shape, and large deflections) must then be solved. The surveys by Edwards and Thomas³ and Ballhaus and Bridgeman⁴ review recent computational developments in the field of transonic aeroelasticity. Some of these developments include modelling of the Navier-Stokes equations⁵ and the Euler equations⁶ for flutter analysis. Application of these higher order formulations, however, has primarily been limited to two-dimensional configurations, due to the

large computational costs incurred. Certain assumptions regarding the flow can be made to yield reduced order formulations such as the full-potential equation⁷ and the computationally efficient transonic small-disturbance (TSD) equation. Research efforts involving the TSD formulation include the development of the XTRAN3S code⁸, the work by Yang, Guruswamy, and Striz⁹, and many others.

A transonic aerodynamics code known as CAP-TSD (Computational Aeroelasticity Program-Transonic Small Disturbance) has been developed at the NASA - Langley Research Center (LaRC). CAP-TSD is capable of handling multiple lifting surfaces with control surfaces, bodies (nacelles, pylons, stores), vertical surfaces, and a fuselage, and solves the TSD equation using an efficient approximate factorization scheme¹⁰. References 11-12 verified the code's ability to accurately predict steady and unsteady pressures for wings and configurations at subsonic, transonic, and supersonic Mach numbers. Flutter prediction using CAP-TSD for two thin, swept-and-tapered wings compared well with experimental flutter results¹³.

The goal of the present study was to update the transonic aeroelastic analysis of the Active Flexible Wing (AFW) wind-tunnel model^{14,15} that was reported in Ref. 16. The Active Flexible Wing (Fig. 1) model is a full-span, sting-mounted wind-tunnel model designed and built by the Rockwell International Corporation. The main goal of the AFW project was to design, implement and validate digital control laws for flutter suppression¹⁴ with simultaneous roll maneuvers with load alleviation. Knowledge of possible regions of instability was, therefore, crucial.

This paper first presents the computational procedures incorporated in CAP-TSD. This includes a brief description of the TSD formulation and the coupled aerodynamic and structural equations of motion that are integrated in time. These equations are used for both static aeroelastic and dynamic analyses of the AFW. An important conclusion of the studies by Yates, Wynne, and Farmer¹⁷ and Yates and Chu¹⁸ was that the accuracy of the transonic flutter prediction is highly dependent on the

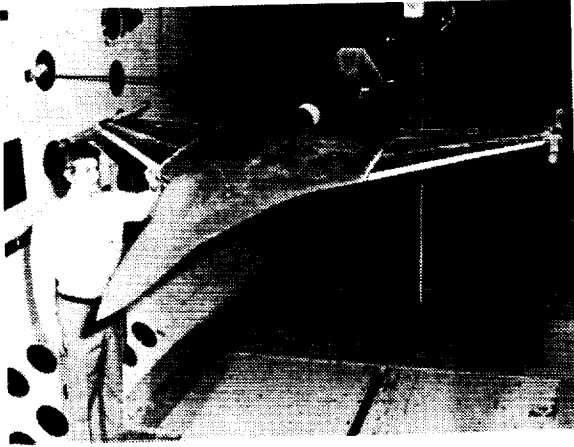


Figure 1 The AFW in NASA-LaRC's Transonic Dynamics Tunnel (TDT).

accuracy of the static aeroelastic state of the wing. As a result, a procedure for computing static aeroelastic deformations¹⁶ is applied to the AFW computational model. The dynamic behavior is computed as a perturbation about previously computed static aeroelastic solutions. The resultant dynamic time histories of the generalized displacements are then analyzed using a modal identification technique to estimate the stability parameters (damping and frequency) of the system at a given Mach number and dynamic pressure. Dynamic results are presented in the form of flutter boundaries, in terms of Mach number and flutter dynamic pressure. Flutter boundaries that account for a corrected modeling of the wing tip ballast store of the AFW, an updated set of mode shapes and frequencies, vorticity and entropy corrections, and a subsonic antisymmetric flutter result are presented and compared with experimental flutter results.

3. COMPUTATIONAL PROCEDURES

In this section, an overview of the computational procedures is presented including a description of the CAP-TSD program, the aeroelastic equations of motion, the time-marching solution of these equations, and the modal identification of the resulting free decay transients.

3.1 CAP-TSD Program

The CAP-TSD program is a finite-difference program which solves the general-frequency modified transonic small-disturbance (TSD) equation. The TSD potential equation is defined by

$$M_\infty^2 (\phi_t + 2\phi_x)_t = [(1 - M_\infty^2)\phi_x + F\phi_x^2 + G\phi_y^2]_x + (\phi_y + H\phi_x\phi_y)_y + (\phi_z)_z \quad (1)$$

where M_∞ is the freestream Mach number, ϕ is the disturbance velocity potential, and the subscripts of ϕ represent partial derivatives.

Several choices are available for the coefficients F , G , and H depending upon the assumptions used in deriving the TSD equation. For transonic applications, the coefficients are herein defined as

$$\begin{aligned} F &= -\frac{1}{2}(\gamma + 1)M_\infty^2, \\ G &= \frac{1}{2}(\gamma - 3)M_\infty^2, \\ H &= -(\gamma - 1)M_\infty^2 \end{aligned} \quad (2)$$

where γ is the ratio of specific heats. The linear potential equation is recovered by simply setting F , G , and H equal to zero.

Equation (1) is solved within CAP-TSD by a time-accurate approximate factorization (AF) algorithm developed by Batina¹⁰. In Refs. 11 to 13, the AF algorithm was shown to be efficient for application to steady or unsteady transonic flow problems. It can provide accurate solutions in only several hundred time steps yielding a significant computational cost savings when compared to alternative methods. Several algorithm modifications have been made which improve the stability of the AF algorithm and the accuracy of the results^{19,20}. One of these improvements is the option to include vorticity and entropy corrections²⁰ for improved shock modelling. The effect of these corrections on the transonic flutter boundary of the AFW model is investigated and presented in a subsequent section of this paper.

The CAP-TSD program can treat configurations with combinations of lifting surfaces and bodies including canard, wing, tail, control surfaces, tip launchers, pylons, fuselage, stores, and nacelles. The configuration capability of the current version of CAP-TSD permits the calculation of pressures on the fuselage and bodies. In the version of CAP-TSD used in this study, modal perturbations of the fuselage and bodies are not included in the boundary conditions and the integration of the pressures on the fuselage and bodies (for computation of the generalized aerodynamic forces) is not included in the aeroelastic solution. However, the aerodynamic influence of both the fuselage and wing tip body of the AFW model are included as interference effects upon the wing pressures.

3.2 Equations of Motion

The aeroelastic equations of motion are based on a right-hand orthogonal coordinate system with the x-direction defined as positive downstream, y-direction positive out the right wing, and the z-direction positive upward. The equations of motion may be written as

$$M\ddot{q} + C\dot{q} + Kq = Q \quad (3)$$

where q is a vector of generalized displacements, M is the generalized mass matrix, C is the generalized damping matrix, and K is the generalized stiffness matrix. Q is the vector of generalized forces where its elements are defined by

$$Q_i = \frac{\rho U^2}{2} c_r^2 \int_s \frac{\Delta p h_i}{\rho U^2/2} \frac{dS}{c_r^2}$$

and Δp is the lifting pressure, ρ is the fluid density, c_r is the root chord, U is the freestream velocity, S is the area of the lifting surface(s) and h_i is the vibration mode shape. Equation (3) is rewritten as

$$\ddot{q} = -M^{-1} Kq - M^{-1} C\dot{q} + M^{-1} Q \quad (4)$$

to permit integration of the equation with respect to time.

3.3 Time-Marching Aeroelastic Solution

The aeroelastic solution procedure implemented within CAP-TSD for integrating Eq. (4) is similar to that described by Edwards, Bennett, Whitlow, and Seidel²¹. Equation (4) is composed of normal mode equations which may be expressed in linear, first-order state-space form as

$$\dot{x}_i = Ax_i + Bu_i \quad (5)$$

where

$$x_i = [q_i \quad \dot{q}_i]^T$$

and

$$A = \begin{bmatrix} 0 & 1 \\ -m_i^{-1} k_i & -m_i^{-1} c_i \end{bmatrix}$$

$$B = m_i^{-1} \frac{\rho U^2}{2} c_r^2 \begin{bmatrix} 0 \\ 1 \end{bmatrix}$$

$$u_i = \int_s \Delta C_p h_i dS / c_r^2$$

$$\Delta C_p = \frac{\Delta p}{\rho U^2/2}$$

In these definitions, m_i , c_i , and k_i are elements of the mass, damping, and stiffness matrices, respectively, corresponding to mode i . The analytical solution to Eq. (5) and a description of its numerical implementation in CAP-TSD is found in Refs. 13 and 21.

For aeroelastic analysis, two steps are generally required in performing the calculations. In the first step, the

steady-state flow field is calculated to account for wing thickness, camber, mean angle of attack, and static aeroelastic deformation, thus providing the starting flow field for the dynamic aeroelastic analysis. Previously published CAP-TSD flutter studies analyzed only symmetric airfoils at zero angle of attack¹³, thereby avoiding the problem of static aeroelastic deformations. For the AFW, the airfoil sections are not symmetric and are rigged at a non-zero angle of attack, so a procedure for computing static aeroelastic solutions had to be developed before an accurate dynamic analysis could be performed. The dynamic analysis would then be a perturbation about a converged static aeroelastic solution at each Mach number and dynamic pressure of interest.

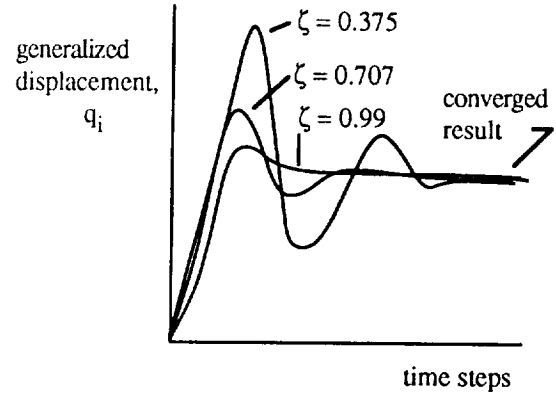


Fig. 2 Convergence of generalized displacements for different values of viscous damping.

The procedure developed¹⁶ and applied in this study for computing static aeroelastic deformations is to allow the structure and aerodynamics to interact with no initial excitation (no initial deflection or velocity) and with a large value of viscous damping to prevent divergence of the solution. This method resulted in convergence of the generalized displacements. Static aeroelastic deformations should be independent of viscous damping and so different values of viscous damping ($\zeta = .375$, $.707$, and $.99$) were evaluated. A typical result for this type of analysis is presented in Fig. 2, which shows a representative variation of a generalized displacement as a function of computational time steps for the three values of viscous damping. It is clear from Fig. 2 that the convergence is indeed independent of the value of viscous damping. Furthermore, the larger the value of viscous damping, the faster the convergence. Therefore, the highest value of viscous damping ($\zeta = 0.99$) was used in order to accelerate the static aeroelastic solution. For the applications presented herein, 2000- 4000 time steps were used to converge the static aeroelastic solutions. An interesting result of this procedure was that it allowed the computation of static aeroelastic deformations at dynamic pressures above the flutter dynamic pressure for the AFW.

Once converged static aeroelastic solutions were computed, the next step was to prescribe an initial disturbance to begin the dynamic structural integration. Disturbance (or modal) velocities in the first three modes were used as initial perturbations. About 7 cycles of the lowest frequency (first) mode were needed for accurate modal identification. For a constant, non-dimensional time step of .01, this required 8000 time steps. In determining a flutter point, the freestream Mach number, M_∞ , and the associated freestream speed, U , were held fixed. A value of the dynamic pressure $\rho U^2/2$ is then used and free decay transients are computed. These resulting transients of the generalized coordinates are analyzed for their content of damped or growing sine-waves, with the rates of growth or decay indicating whether the dynamic pressure is above or below the flutter value. This analysis then indicates whether to increase or decrease the value of dynamic pressure in subsequent runs to determine a neutrally stable result.

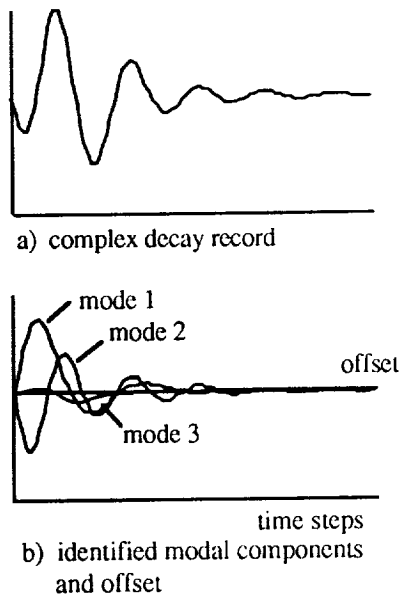


Fig. 3 Example of dynamic decay record and its modal components.

3.4 Modal Identification

As previously mentioned, CAP-TSD generates free decay transients that must be analyzed for the modal stability characteristics. A typical transient for the AFW model, calculated using CAP-TSD is shown in Fig. 3(a). The first three modes used in the analysis were excited by specifying an initial condition for each modal velocity to produce a complex decay record. This record is analyzed using a least-squares curve-fit of the response data with complex exponential functions. The program utilized is a derivative of the one described in Ref. 22. The components of the transient of Fig. 3(a) are plotted in Fig. 3(b) to the same scale. The free decay properties of each mode for this condition are readily apparent and the

mean or offset value is the static aeroelastic deformation of the mode being analyzed. A sufficient range of dynamic pressure must be considered to determine all relevant flutter points.

4. ANALYSIS AND RESULTS

4.1 CAP-TSD Computational Model

The AFW geometry data was obtained from Rockwell International, including detailed airfoil shape information. From this geometry data two computational models of the AFW were generated. A half-span model, with symmetry specified at the centerline, was used for symmetric analyses and a full-span model was used for antisymmetric analyses. Both computational models consist of a fuselage, the addition of the region aft of the main wing and next to the fuselage referred to as the coat-tail, the main wing(s) with all four control surfaces per wing, and the wing tip ballast store(s). The grid dimensions for the half-span model are 134x51x62 in the x-, y-, and z-directions respectively for a total of 423,708 grid points. The grid extends 10 root chords upstream, 10 root chords downstream, 2 semi-span lengths in the y-direction, and 10 root chords in the positive and negative z-direction. The full-span grid is dimensioned 134x101x62 grid points in the x-, y-, and z-directions (839,108 grid points). The wind-tunnel sting mount is modeled by extending the computational fuselage aft to the downstream boundary of the grid. The grid density is increased in regions where large changes in the flow are expected, such as at the leading edge, trailing edge, wing tip, and control-surface sides and hinge lines. The four control surfaces per wing are the leading-edge inboard (LEI), leading-edge outboard (LEO), trailing-edge inboard (TEI), and trailing-edge outboard (TEO). Each control surface has a chord that is 25% of the local chord and a span that is 28% of the semi-span. The airfoil definition includes the control surface actuator bumps on the outboard half of the wing. There are slight surface discontinuities on the wind-tunnel model where the wing box and control surfaces meet (at the quarter- and three-quarter chord). These discontinuities

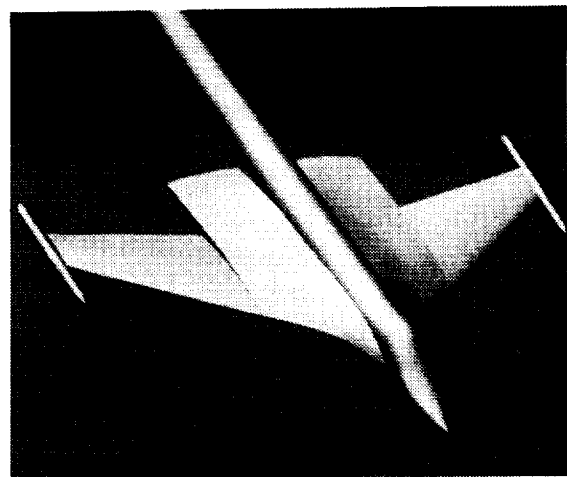


Fig. 4 CAP-TSD computational model of the AFW.

are not included in the analytical model because of potential numerical difficulties. The effect of the actuator bumps and the control surface/wing box discontinuities on the measured and computed static pressure distributions will be presented in a subsequent section. A computer-generated picture of the CAP-TSD model of the AFW is shown in Fig. 4. Although not shown in the figure, a protrusion on the underside of the fuselage that houses the model's pitch actuator is also included in the analytical model.

Analytical modes and frequencies were obtained from a finite-element model, that includes the mass of the tip ballast store, and separated into symmetric and antisymmetric modal data sets. The flutter analyses of Ref. 16 were performed using analytical mode shapes with measured frequencies (ground vibration test). The symmetric data was shown by linear analysis¹⁴ to be the most flutter critical in the higher, subsonic Mach number regime and so only symmetric motions were analyzed in Ref. 16 using the semi-span model. Since then, an updated set of symmetric and antisymmetric mode shapes have been generated based on experimental data. These updated mode shapes are defined at a denser set of structural node points for improved accuracy in the interpolation procedure. The interpolation of mode shape displacements and slopes at the computational grid points is done via a surface spline²³. Each structural section was splined separately and then recombined to form the necessary input to CAP-TSD. The separate structural sections are the wing box, coat-tail, and the four control surfaces. Slender bodies such as the fuselage and tip ballast store are not given any modal definition in CAP-TSD, as was previously mentioned, therefore no modal data were needed for these components.

4.2 Static Aeroelastic Results

The accuracy of the static aeroelastic solution was investigated in Ref. 16 by comparing analytical results, using the original set of symmetric mode shapes, with existing experimental data. Two sets of experimental data from previous AFW tests in a heavy gas were used for this purpose. These data included : 1) pressure coefficient distributions and 2) control-surface effectiveness parameters. In Ref. 16, by comparing calculated and experimental pressure distributions at a chosen Mach number and dynamic pressure, it was concluded that the static aeroelastic procedure provided reasonable estimates of the static aeroelastic deformation of the AFW using the original set of mode shapes. It was also concluded that comparisons between the calculated and experimental control surface effectiveness parameters were qualitatively reasonable but were deficient quantitatively due to the lack of viscous effects in the CAP-TSD model. Therefore, in the present study, the accuracy of the static aeroelastic procedure is not reassessed, but instead only a comparison of calculated pressure distributions using the updated set of mode shapes and the experimental pressure distributions is presented. It should be mentioned that the AFW configuration for these previous tests did not include the tip ballast store used in the recent test so that in order for the CAP-TSD calculations to compare with the earlier experiments, the tip ballast store was deleted from the computational model and the tip fairing was added.

4.2.1 Pressure distributions

Figure 5 presents pressure coefficient distributions versus percent chord for CAP-TSD with the updated set of mode shapes and experiment at $M = 0.9$ and a dynamic pressure, q , of 150 psf (7.18 kPa) at the three spanwise stations shown.

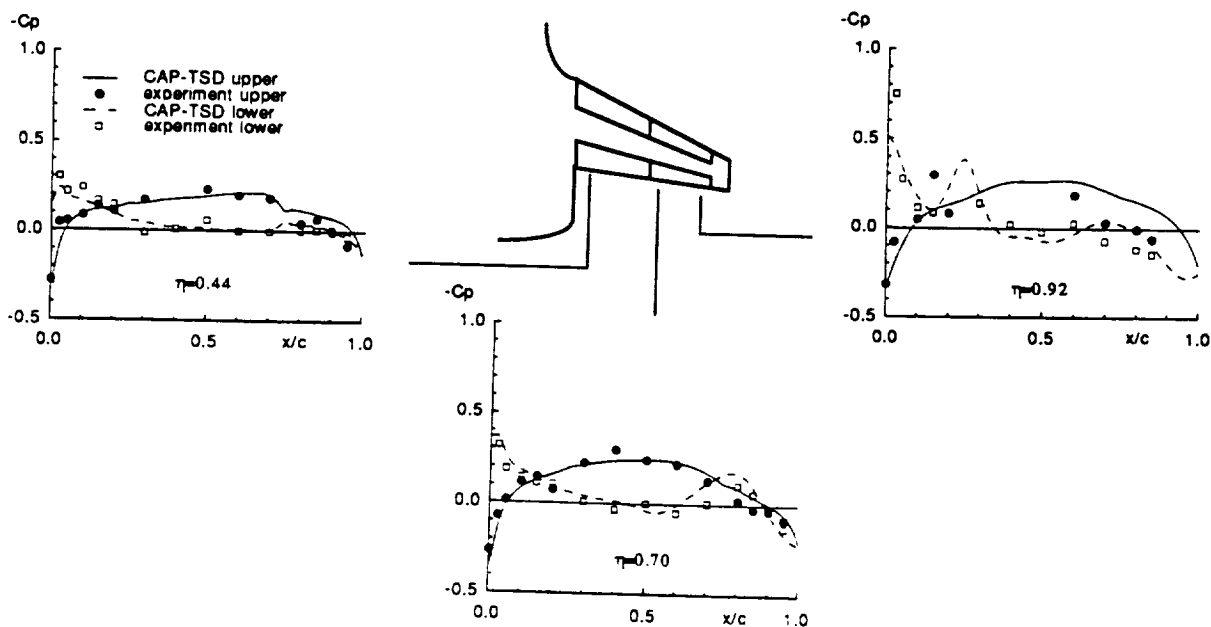


Fig. 5 Pressure distributions at $M=0.9$ and $q=150$ psf in a heavy gas.

As with the original set of mode shapes, the overall agreement between the most recent analysis and experiment is good, with some discrepancies occurring near the trailing edge and wing tip. The first two span stations compare reasonably well from the leading edge up to about sixty percent of the local chord. Sudden changes in the experimental data can be seen near the quarter-chord at the second span station and near the three-quarter chord for all three span stations. These disruptions in the flow may be caused by the previously-mentioned physical discontinuities where wing box and control surfaces meet. At the second and third span stations, the effect of the actuator bumps on the lower surface pressures is evident. Agreement between analysis and experiment deteriorates at the third span station, possibly due to separated and/or tip vortex flow around the wing tip region.

Comparisons of the static aeroelastic results using the updated structural model with those of the previous model of Ref. 16 show essentially the same behavior. There exists a slight difference between the two results at the first span station near the three-quarter chord location where the updated structural model reveals the presence, or beginnings of, a shock that was not present with the original structural model. This appears to be a slight improvement in comparison with the test data. However, the exact cause of the sudden change in the experimental pressure distribution at this location is not clear as it may be due to a shock or to the geometric discontinuity that exists at the quarter-chord and three-quarter chord locations of the wing.

4.3 Dynamic Results

4.3.1 Symmetric motions

Flutter boundaries were computed at $M=0.5, 0.9, 0.92, 0.93, 0.94$, and 0.95 . The analyses that included the vorticity and entropy corrections were computed at $M=0.5, 0.9, 0.92, 0.93$, and 0.95 . Although the results for all of these Mach numbers are included in the figures, results are discussed primarily for the $M=0.5, 0.9, 0.93$, and 0.95 cases. All flutter analyses are for the AFW model in air at 1.5 degrees angle of attack and including a viscous damping of 0.015 (structural damping of 0.03).

4.3.1.1 Corrected tip store modeling

In Ref. 16, a rather severe transonic flutter dip was computed using the CAP-TSD code and the bottom of this computational transonic flutter dip did not agree well with the experimental transonic flutter dip. Figure 6, from Ref. 16, is a comparison of the CAP-TSD computed flutter boundary, the linear flutter boundary defined using the doublet lattice theory²⁴, and the experimental flutter results from the fall of 1989 and the spring of 1991 wind-tunnel tests. Accounting for nonlinearities in the flow, by the application of the CAP-TSD code, is a clear improvement over the linear flutter predictions. The no-flutter track, shown in the figure, is the path, in terms of Mach number and dynamic pressure, through which the wind tunnel proceeds for which no experimental flutter was encountered. This no-flutter track therefore defines a

lower bound for the bottom of the experimental transonic flutter dip which disagrees with the CAP-TSD predicted bottom of the transonic flutter dip. As a result, one of the goals of the present study was to investigate some of the possible causes of this discrepancy by modifying and improving specific elements of the analysis.

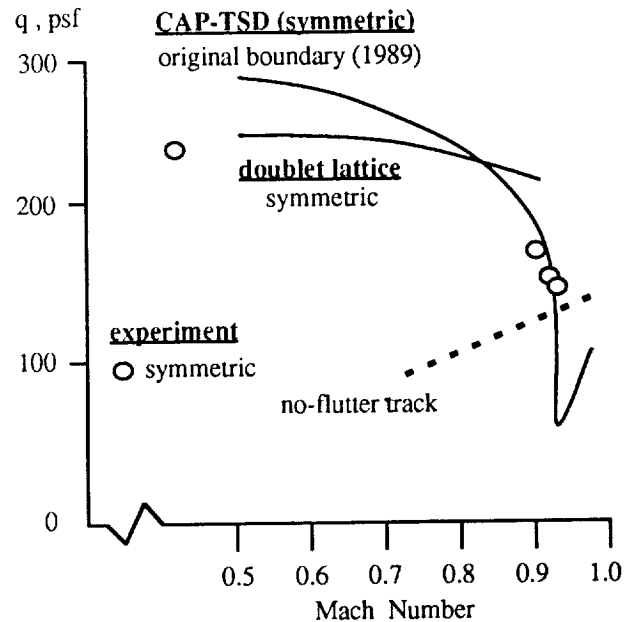


Fig. 6 Comparison of linear, nonlinear and experimental flutter boundaries for original mode shapes (Ref. 16).

The first improvement to the analysis was the correction of an error in the modeling of the wing tip ballast store. The error consisted of a sign change in a portion of the slopes that geometrically define the wing tip ballast store. The effect of this error was investigated and the resultant flutter boundary for the corrected wing tip ballast store model is presented in Fig. 7 along with the original, uncorrected flutter boundary presented in Fig. 6. At $M = 0.5$, the effect of the corrected tip store model was to reduce the flutter dynamic pressure from 290 psf (13.89 kPa) to 259 psf (12.40 kPa) with a change in flutter frequency from 10.70 Hz to 11.20 Hz. There was no change in the flutter mechanism at this Mach number from the mechanism reported in Ref. 16, which consisted of a classical coalescence of the first-bending mode and the first-torsion mode. The flutter dynamic pressure dropped only slightly at $M=0.9$ from 190 psf (9.10 kPa) to 182 psf (8.71 kPa) while at $M=0.93$ the flutter dynamic pressure increased from 52 psf (2.49 kPa) to 77 psf (3.69 kPa). The flutter dynamic pressure at $M=0.95$ increased significantly from 81 psf (3.88 kPa) to 133 psf (6.37 kPa). Again, the flutter mechanism for these three transonic Mach numbers was essentially the same as the mechanism reported in Ref. 16 for transonic Mach numbers, which consisted of a first-bending-dominated instability. The changes in flutter frequency at $M=0.9, M=0.93$, and $M=0.95$ were, respectively, from 9.50 Hz to

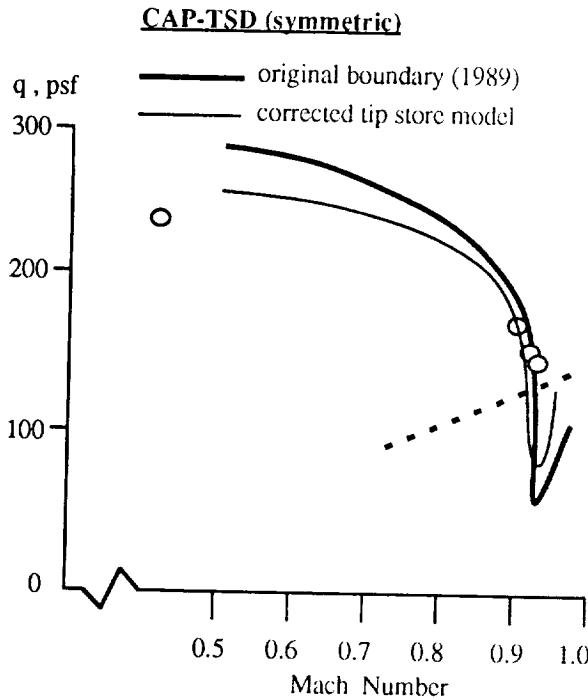


Fig. 7 The effect of the corrected tip store modeling using the original mode shapes.

9.36 Hz, from 7.78 Hz to 8.08 Hz, and from 8.07 Hz to 8.83 Hz.

The corrected modeling of the wing tip ballast store therefore improved the subsonic flutter boundary by lowering the flutter dynamic pressure in the direction of the experimental result while reducing the severity of the computational transonic flutter dip and thereby improving the correlation with the transonic experimental results. These results also indicate the sensitivity of the calculated flutter boundary to modeling of tip aerodynamics at both subsonic and transonic conditions. For all of the results that follow, the corrected modeling of the wing tip ballast store has, of course, been implemented.

4.3.1.2 Updated mode shapes and frequencies

An updated and improved set of mode shapes and frequencies were obtained after the wind-tunnel test of 1989. The improvements consisted of : a) refinements to the structural model based on experimental data and b) a denser set of structural node points for improved mode shape definition, in particular around the control surface regions and the wing tip regions of the AFW.

The flutter boundary due to the updated structural model is shown in Fig. 8 and compared to the flutter boundary due to the original structural model (corrected boundary from Fig. 7). There is an increase in flutter dynamic pressure at $M=0.5$ with the new structural model. The increase in flutter dynamic pressure is from 259 psf (12.40 kPa) to 281 psf (13.45 kPa) with a decrease in flutter frequency

from 11.20 Hz to 10.86 Hz. At $M=0.9$, the flutter dynamic pressure increases from 182 psf (8.71 kPa) to 203 psf (9.72 kPa) with a slight change in flutter frequency from 9.36 Hz to 9.44 Hz. The flutter dynamic pressure at $M=0.93$ increases significantly from 77 psf (3.69 kPa) to 103 psf (4.93 kPa) with an increase in frequency from 8.08 Hz to 8.32 Hz. For $M=0.95$ the flutter dynamic pressure also increases significantly from 133 psf (6.37 kPa) to 183 psf (8.76 kPa) with an increase in flutter frequency from 8.83 Hz to 9.33 Hz.

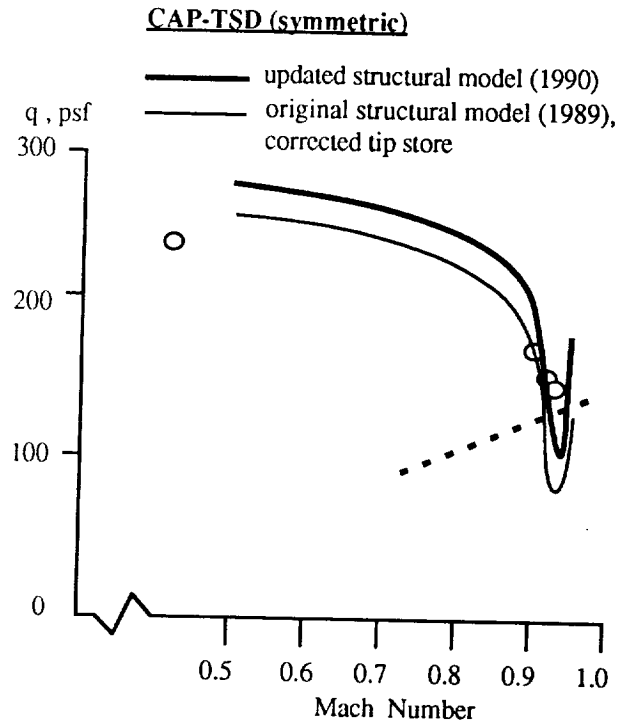


Fig. 8 Comparison of original (corrected) and updated structural models.

The effect of the updated structural model is therefore beneficial at transonic Mach numbers greater than $M=0.9$ since the correlation with the experimental transonic flutter results is improved, but at $M=0.5$ and $M=0.9$ the comparison with experiment is degraded. A possible reason for this deficiency in the CAP-TSD prediction is that the current version of the code treats bodies such as the wing tip ballast store and fuselage as aerodynamic influences with no modal definition. Although the effect of a modally-defined fuselage on the flutter boundary may be minimal, the effect of a modally-defined wing tip ballast store is probably significant as can be seen by the sensitivity to changes in the modeling of the wing tip ballast store in Fig. 7. These effects should be investigated when a version of the CAP-TSD code becomes available that accounts for modal deformations of the fuselage and bodies and thus the contribution of these components to the generalized aerodynamic forces. Viscous effects, not accounted for in the current inviscid

version of the code, may also have a significant effect on both the subsonic and transonic flutter boundaries.

4.3.1.3 Vorticity and entropy corrections

The vorticity and entropy corrections defined in Ref. 20 and incorporated in current versions of the CAP-TSD code were applied with updated mode shapes and frequencies at $M=0.5, 0.9, 0.92, 0.93$, and 0.95 . These corrections typically reduce shock strength and shift the shock location forward. The resultant flutter boundary due to the implementation of these corrections is compared to the transonic portion of the flutter boundary for the updated structural model without vorticity and entropy corrections in Fig. 9. The effect of the corrections at $M=0.9$ is minimal, lowering the flutter dynamic pressure from 203 psf (9.72 kPa) to 200 psf (9.58 kPa) and reducing the flutter frequency from 9.44 Hz to 9.40 Hz. The effects of the corrections are significant at $M=0.93$ where the flutter dynamic pressure increased from 103 psf (4.93 kPa) to 126 psf (6.03 kPa) with an increase in flutter frequency from 8.32 Hz to 8.53 Hz. An interesting effect is noticed at $M=0.95$ where the flutter dynamic pressure is reduced from 183 psf (8.76 kPa) to 130 psf (6.22 kPa) and the flutter frequency drops from 9.33 Hz to 8.60 Hz. The effect of the vorticity and entropy corrections therefore is significant in that it improves the correlation with experiment at the transonic Mach numbers evaluated. The inclusion of vorticity and entropy also tends to widen the rather steep and narrow transonic flutter dip previously computed (Figs. 6, 7, and 8).

In general, for symmetric motions, the effects of improved and updated analyses results in excellent agreement with experiment at transonic conditions while resulting in some degradation of the comparisons at $M=0.5$ and $M=0.9$. It is possible that accounting for the modal definition of the wing tip ballast store will provide some insight into this discrepancy. It is also interesting to note that the computational result at $M=0.92$ is insensitive to the computational modifications and improvements described above and compares extremely well with experiment. At this Mach number, the calculated flutter dynamic pressure, for the vorticity and entropy case, for example, is 151 psf (7.23 kPa) which differs only slightly from the experimental flutter value of 156 psf (7.47 kPa).

4.3.2 Antisymmetric motions

In order to generate antisymmetric aeroelastic responses, a full-span model of the AFW was generated. A progressive verification of the full-span model and of the CAP-TSD code's capability for handling full-span aeroelastic analyses was deemed necessary before any antisymmetric flutter analyses were performed. This progressive verification proceeded as follows. First, a full-span, rigid and steady solution was compared to a semi-span, rigid and steady solution at the same Mach number. Lift and moment coefficients for both cases were identical, thereby verifying the aerodynamic modeling of the full-span model and the accurate implementation of the symmetric boundary condition for the semi-span model. Second, static aeroelastic solutions were

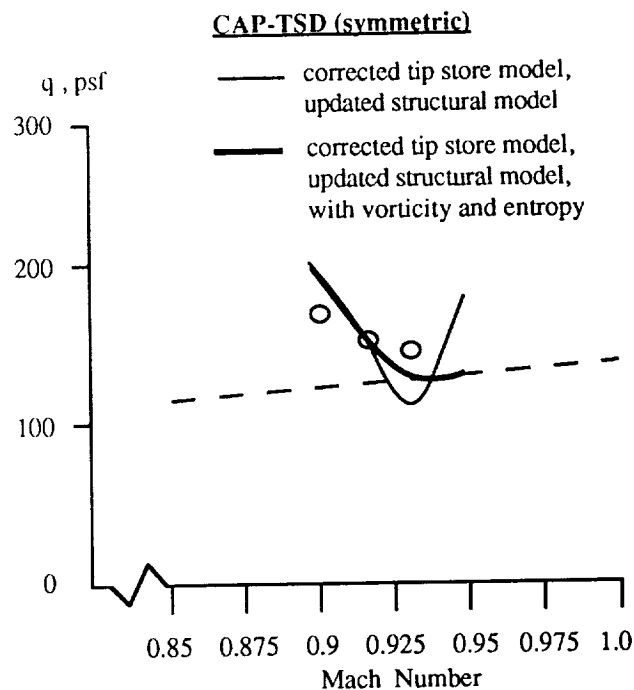


Fig. 9 Comparison of transonic computational and experimental flutter boundaries for updated structural model with and without vorticity and entropy corrections.

computed for both models using symmetric modes at a chosen Mach number and dynamic pressure. Again, the resultant lift and moment coefficients including static aeroelastic deformation of both models were in exact agreement, verifying the modal definition of the full-span model. Finally, a full-span, symmetric dynamic analysis was compared to a semi-span, symmetric dynamic analysis resulting in identical transients, verifying the full-span model for dynamic analyses.

An important aspect of the antisymmetric flutter analyses is the necessary addition of symmetric mode shapes to the aeroelastic modeling along with the antisymmetric mode shapes. The reason for this is that since dynamic analyses are computed about converged static aeroelastic solutions and since static aeroelastic solutions are symmetric for a vehicle defined symmetrically about its centerline, antisymmetric dynamic analyses require the inclusion of symmetric modes as well. The computational model therefore consists of ten symmetric modes needed for static aeroelastic solutions and ten antisymmetric modes needed for the dynamic aeroelastic solutions. These additional modes do not increase the computer time significantly as the finite-difference aerodynamics dominate the CPU time.

An antisymmetric computational flutter point has been obtained for the $M=0.5$ case thus far. Figure 10 is a comparison of the linear symmetric and antisymmetric flutter boundaries computed using the doublet lattice unsteady aerodynamic theory for the updated set of mode

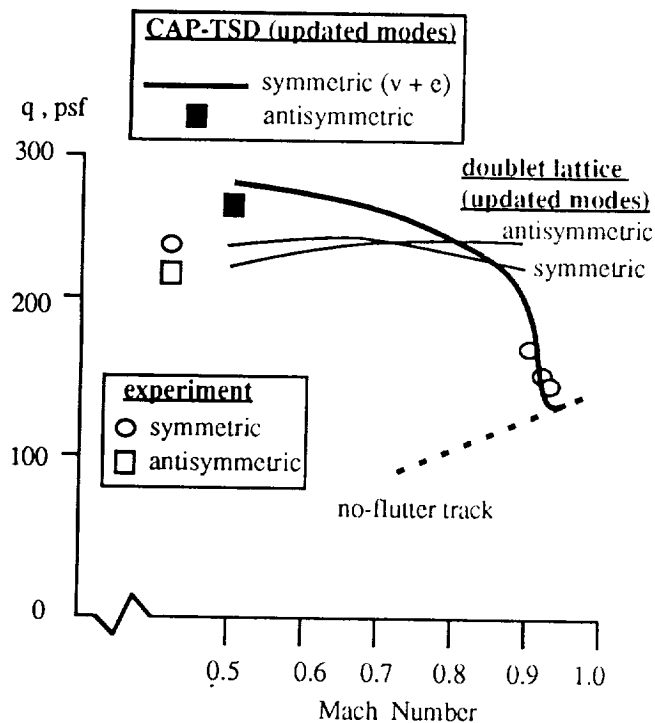


Fig. 10 Comparison of linear and nonlinear flutter boundaries for the updated symmetric (with vorticity and entropy) and anti-symmetric structural model and experimental results.

shapes²⁴, the CAP-TSD symmetric flutter boundary for the updated set of mode shapes with vorticity and entropy (Fig. 9), the CAP-TSD antisymmetric flutter result at $M=0.5$, and the symmetric and antisymmetric experimental flutter points. Although the CAP-TSD predicted antisymmetric flutter dynamic pressure of 272 psf (13.02 kPa) is significantly higher than the experimental value of 219 psf (10.49 kPa), the CAP-TSD analyses indicate that the antisymmetric instability is lower in flutter dynamic pressure than the symmetric instability at $M=0.5$ (dynamic pressure of 281 psf (13.45 kPa)). This is consistent with the doublet lattice symmetric and antisymmetric results and the experimental symmetric and antisymmetric results. The discrepancy between the CAP-TSD results at $M=0.5$ and the subsonic experimental flutter results (and the doublet lattice results as well) may be due to the lack of modal definition of the wing tip ballast store and thus its contribution to the unsteady generalized forces in the CAP-TSD computations. The effect of a modally-defined wing tip ballast store on the subsonic and transonic CAP-TSD flutter boundaries still needs to be investigated. Furthermore, viscous effects have not been addressed by the analyses presented thus far and need to be investigated as well.

5. CONCLUDING REMARKS

The goals of this study were to update the calculated symmetric aeroelastic behavior of the AFW wind-tunnel

model using the CAP-TSD code, to evaluate the full-span, antisymmetric aeroelastic capability of the code, and to compare the results with experimental flutter data.

A static aeroelastic procedure previously developed was applied to an updated structural model. Results compared favorably with experimental pressure data from a previous AFW wind tunnel test. Static aeroelastic solutions therefore provided reasonable estimates of the static aeroelastic deformation of the wing. Dynamic analyses were then performed as perturbations about converged static aeroelastic solutions.

The updated dynamic analyses consisted of modifications and improvements to key elements of the aeroelastic modelling. These modifications and improvements include a corrected aerodynamic modelling of the wing tip ballast store, an updated structural model, and the addition of vorticity and entropy corrections.

The corrected modelling of the wing tip ballast store resulted in improved correlation with subsonic and transonic symmetric experimental flutter points. The significant sensitivity of the aeroelastic analyses to changes in the modelling of the wing tip ballast store was revealed. The updated structural model improved the correlation with experiment at transonic Mach numbers but degraded the correlation with experiment at the subsonic condition. The addition of vorticity and entropy corrections provided further improvements in the correlation with experiment at transonic Mach numbers. This is an indication of the importance of including vorticity and entropy effects in the computations.


A full-span computational model of the AFW was generated and used for generating an antisymmetric flutter point at $M=0.5$. Deficiencies in the correlation with experiment at this Mach number may be due to the lack of modal definition in the aerodynamics of the wing tip ballast store, which might have a significant effect on the generalized aerodynamic forces of the vehicle. Viscous effects, not accounted for in this inviscid version of the CAP-TSD code, may also play an important role in both the subsonic and transonic regimes.

6. ACKNOWLEDGEMENT

The authors would like to thank B. Perry III of the Aeroservoelasticity Branch and S. R. Cole of the Configuration Aeroelasticity Branch for providing experimental flutter data.

7. REFERENCES

- ¹Isogai, K. : On the Transonic-Dip Mechanism of Flutter of a Sweptback Wing. *AIAA Journal*, Volume 17, Number 7, July 1979, pp. 793-795.
- ²Davis, S. S.; and Malcolm, G. N. : Experiments in Unsteady Transonic Flow. AIAA Paper Number 79-0769, AIAA/ASME/ASCE/AHS 20th Structures, Structural Dynamics, and Materials Conference, St. Louis, MO, April 4-6, 1979.

 Report Documentation Page			
1. Report No. NASA TM-104142		2. Government Accession No.	
4. Title and Subtitle Investigation of the Aeroelastic Stability of the AFW Wind-Tunnel Model Using CAP-TSD		3. Recipient's Catalog No.	
		5. Report Date September 1991	
7. Author(s) Walter A. Silva and Robert M. Bennett		6. Performing Organization Code	
		8. Performing Organization Report No.	
9. Performing Organization Name and Address NASA Langley Research Center Hampton, Virginia 23665-5225		10. Work Unit No. 509-10-02-03	
		11. Contract or Grant No.	
12. Sponsoring Agency Name and Address National Aeronautics and Space Administration Washington, DC 20546-0001		13. Type of Report and Period Covered Technical Memorandum	
		14. Sponsoring Agency Code	
15. Supplementary Notes This paper is to be presented at the AGARD Specialists Meeting in San Diego, California, on October 6-11, 1991.			
16. Abstract The CAP-TSD (Computational Aeroelasticity Program - Transonic Small Disturbance) code, developed at the NASA Langley Research Center, is applied to the Active Flexible Wing (AFW) wind-tunnel model for prediction of the model's transonic aeroelastic behavior. A semi-span computational model is used for evaluation of symmetric motions and a full-span model is used for evaluation of antisymmetric motions. Static aeroelastic solutions using CAP-TSD are computed. Dynamic (flutter) analyses are then performed as perturbations about the static aeroelastic deformations and presented as flutter boundaries in terms of Mach number and dynamic pressure. Flutter boundaries that take into account modal refinements, vorticity and entropy corrections, antisymmetric motions and sensitivity to the modeling of the wing tip ballast stores are also presented and compared with experimental flutter results.			
17. Key Words (Suggested by Author(s)) Transonic Aeroelasticity CAP-TSD Active Flexible Wing Flutter		18. Distribution Statement Unclassified - Unlimited Subject Category 02	
19. Security Classif. (of this report)	20. Security Classif. (of this page)	21. No. of pages	22. Price

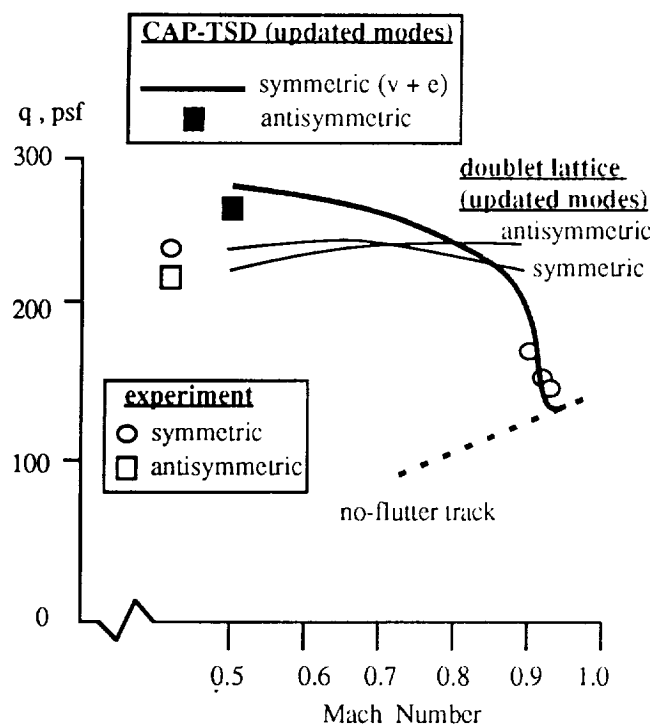


Fig. 10 Comparison of linear and nonlinear flutter boundaries for the updated symmetric (with vorticity and entropy) and anti-symmetric structural model and experimental results.

shapes²⁴, the CAP-TSD symmetric flutter boundary for the updated set of mode shapes with vorticity and entropy (Fig. 9), the CAP-TSD antisymmetric flutter result at $M=0.5$, and the symmetric and antisymmetric experimental flutter points. Although the CAP-TSD predicted antisymmetric flutter dynamic pressure of 272 psf (13.02 kPa) is significantly higher than the experimental value of 219 psf (10.49 kPa), the CAP-TSD analyses indicate that the antisymmetric instability is lower in flutter dynamic pressure than the symmetric instability at $M=0.5$ (dynamic pressure of 281 psf (13.45 kPa)). This is consistent with the doublet lattice symmetric and antisymmetric results and the experimental symmetric and antisymmetric results. The discrepancy between the CAP-TSD results at $M=0.5$ and the subsonic experimental flutter results (and the doublet lattice results as well) may be due to the lack of modal definition of the wing tip ballast store and thus its contribution to the unsteady generalized forces in the CAP-TSD computations. The effect of a modally-defined wing tip ballast store on the subsonic and transonic CAP-TSD flutter boundaries still needs to be investigated. Furthermore, viscous effects have not been addressed by the analyses presented thus far and need to be investigated as well.

5. CONCLUDING REMARKS

The goals of this study were to update the calculated symmetric aeroelastic behavior of the AFW wind-tunnel

model using the CAP-TSD code, to evaluate the full-span, antisymmetric aeroelastic capability of the code, and to compare the results with experimental flutter data.

A static aeroelastic procedure previously developed was applied to an updated structural model. Results compared favorably with experimental pressure data from a previous AFW wind tunnel test. Static aeroelastic solutions therefore provided reasonable estimates of the static aeroelastic deformation of the wing. Dynamic analyses were then performed as perturbations about converged static aeroelastic solutions.

The updated dynamic analyses consisted of modifications and improvements to key elements of the aeroelastic modelling. These modifications and improvements include a corrected aerodynamic modelling of the wing tip ballast store, an updated structural model, and the addition of vorticity and entropy corrections.

The corrected modelling of the wing tip ballast store resulted in improved correlation with subsonic and transonic symmetric experimental flutter points. The significant sensitivity of the aeroelastic analyses to changes in the modelling of the wing tip ballast store was revealed. The updated structural model improved the correlation with experiment at transonic Mach numbers but degraded the correlation with experiment at the subsonic condition. The addition of vorticity and entropy corrections provided further improvements in the correlation with experiment at transonic Mach numbers. This is an indication of the importance of including vorticity and entropy effects in the computations.

A full-span computational model of the AFW was generated and used for generating an antisymmetric flutter point at $M=0.5$. Deficiencies in the correlation with experiment at this Mach number may be due to the lack of modal definition in the aerodynamics of the wing tip ballast store, which might have a significant effect on the generalized aerodynamic forces of the vehicle. Viscous effects, not accounted for in this inviscid version of the CAP-TSD code, may also play an important role in both the subsonic and transonic regimes.

6. ACKNOWLEDGEMENT

The authors would like to thank B. Perry III of the Aeroservoelasticity Branch and S. R. Cole of the Configuration Aeroelasticity Branch for providing experimental flutter data.

7. REFERENCES

¹Isogai, K. : On the Transonic-Dip Mechanism of Flutter of a Sweptback Wing. *AIAA Journal*, Volume 17, Number 7, July 1979, pp. 793-795.

²Davis, S. S.; and Malcolm, G. N. : Experiments in Unsteady Transonic Flow. AIAA Paper Number 79-0769, AIAA/ASME/ASCE/AHS 20th Structures, Structural Dynamics, and Materials Conference, St. Louis, MO, April 4-6, 1979.

- ³Edwards, J. W.; and Thomas, J. L. : Computational Methods for Unsteady Transonic Flows, Chapter 5 in Unsteady Transonic Aerodynamics, Edited by David Nixon, Progress in Astronautics and Aeronautics, Volume 120, 1989.
- ⁴Ballhaus, W. F.; and Bridgeman, J. O. : Numerical Solution Techniques for Unsteady Transonic Problems. AGARD Report Number 679, Paper Number 16, March 1980.
- ⁵Wu, J. C. ; Kaza, K. R. V.; and Sankar, N. L. : A Technique for the Prediction of Airfoil Flutter Characteristics in Separated Flows. AIAA Paper Number 87-0910, Presented at the AIAA/ASME/ASCE/AHS 28th Structures, Structural Dynamics, and Materials Conference, Monterey, CA, April 6-8, 1987.
- ⁶Bendiksen, O. O.; and Kousen, K. : Transonic Flutter Analysis Using the Euler Equations. AIAA Paper Number 87-0911, Presented at the AIAA/ASME/ASCE/AHS 28th Structures, Structural Dynamics, and Materials Conference, Monterey, CA, April 6-8, 1987.
- ⁷Shankar, V.; and Ide, H. : Unsteady Full Potential Computations Including Aeroelastic Effects. *Proceedings of the 5th International Conference on Numerical Methods in Laminar and Turbulent Flow*, Volume 5, Part 2, Montreal, Canada, July 6-10, 1987.
- ⁸Borland, C. J.; and Rizzetta, D. P. : Nonlinear Transonic Flutter Analysis. *AIAA Journal*, Volume 20, November 1982, pp. 1606-1615.
- ⁹Yang, T. Y.; Guruswamy, P.; and Striz, A. G. : Application of Transonic Codes to Flutter Analysis of Conventional and Supercritical Airfoils. AIAA Paper Number 81-0603, Proceedings of AIAA Dynamics Specialist Conference, Atlanta, GA, April 9-10, 1981, pp. 332-342.
- ¹⁰Batina, J. T. : Efficient Algorithm for Solution of the Unsteady Transonic Small-Disturbance Equation. *Journal of Aircraft*, Volume 25, July 1988, pp. 598-605.
- ¹¹Batina, J. T.; Seidel, D. A.; Bland, S. R.; and Bennett, R. M. : Unsteady Transonic Flow Calculations for Realistic Aircraft Configurations. *Journal of Aircraft*, Volume 26, January 1989, pp. 21-28.
- ¹²Bennett, R. M.; Bland, S. R.; Batina, J. T.; Gibbons, M. D.; and Mabey, D. G. : Calculation of Steady and Unsteady Pressures on Wings at Supersonic Speeds with a Transonic Small-Disturbance Code. AIAA Paper Number 87-0851, Presented at the AIAA/ASME/ASCE/AHS 28th Structures, Structural Dynamics, and Materials Conference, Monterey, CA, April 6-8, 1987.
- ¹³Bennett, R. M.; Batina, J. T.; and Cunningham, H. J. : Wing Flutter Calculations with the CAP-TSD Unsteady Transonic Small-Disturbance Program. *Journal of Aircraft*, Volume 26, Number 9, September 1989, pp. 876 - 882.
- ¹⁴Perry, B. III; Mukhopadhyay, V.; Hoadley, S. T.; Cole, S. R.; Buttrill, C. S.; and Houck, J. A. : Design, Implementation, Simulation, and Testing of Digital Flutter Suppression Systems for the Active Flexible Wing Wind-Tunnel Model. ICAS Paper Number 90-1.3.2, Presented at the 17th International Council of the Aeronautical Sciences, Stockholm, Sweden, September 9-14, 1990.
- ¹⁵Mukhopadhyay, V.; Perry, B. III; and Noll, T. E. : Flutter Suppression Control Law Synthesis for the Active Flexible Wing Model. Paper Number 89-059, Presented at the European Forum on Aeroelasticity and Structural Dynamics, Aachen, FRG, April 17-19, 1989.
- ¹⁶Silva, W. A. ; and Bennett, R. M. : Predicting the Aeroelastic Behavior of a Wind-Tunnel Model Using Transonic Small-Disturbance Theory, ICAS Paper Number 90-1.1.1, Presented at the 17th International Council of the Aeronautical Sciences, Stockholm, Sweden, September 9-14, 1990.
- ¹⁷Yates, E. C. Jr.; Wynne, E. C. ; and Farmer, M. G. : Measured and Calculated Effects of Angle of Attack on the Transonic Flutter of a Supercritical Wing. NASA TM 83276, August 1982.
- ¹⁸Yates, E. C. Jr.; and Chu, L. : Static Aeroelastic Effects on the Flutter of a Supercritical Wing. NASA TM 89132, March 1987.
- ¹⁹Batina, J. T. : Unsteady Transonic Algorithm Improvements for Realistic Aircraft Applications. *Journal of Aircraft*, Volume 26, February 1989, pp. 131-139.
- ²⁰Batina, J. T. : Unsteady Transonic Small-Disturbance Theory Including Entropy and Vorticity Effects. *Journal of Aircraft*, Volume 26, Number 6, June 1989, pp. 531 - 538.
- ²¹Edwards, J. W.; Bennett, R. M.; Whitlow, W. Jr.; and Seidel, D. A. : Time-Marching Transonic Flutter Solutions Including Angle-of-Attack Effects. *Journal of Aircraft*, Volume 20, Number 11, November 1983, pp. 899-906.
- ²²Bennett, R. M.; and Desmarais, R. N. : Curve Fitting of Aeroelastic Transient Response Data with Exponential Functions. *Flutter Testing Techniques*, NASA SP-415, pp. 43-58, May 1975.
- ²³Harder, R. L.; and Desmarais, R. N. : Interpolation Using Surface Splines. *Journal of Aircraft*, Volume 9, February 1972, pp. 189-191.

²⁴ Silva, W. A. ; Heeg, J. ; and Bennett, R. M. : Aeroelastic Modeling of the Active Flexible Wing Wind-Tunnel Model, In NASA CP 10065, Presented at the Fourth NASA Workshop on Computational Control of Flexible Aerospace Systems, Williamsburg, Virginia, July 11-13, 1990.



Report Documentation Page

1. Report No. NASA TM-104142		2. Government Accession No.		3. Recipient's Catalog No.	
4. Title and Subtitle Investigation of the Aeroelastic Stability of the AFW Wind-Tunnel Model Using CAP-TSD				5. Report Date September 1991	
				6. Performing Organization Code	
7. Author(s) Walter A. Silva and Robert M. Bennett				8. Performing Organization Report No.	
				10. Work Unit No. 509-10-02-03	
9. Performing Organization Name and Address NASA Langley Research Center Hampton, Virginia 23665-5225				11. Contract or Grant No.	
				13. Type of Report and Period Covered Technical Memorandum	
12. Sponsoring Agency Name and Address National Aeronautics and Space Administration Washington, DC 20546-0001				14. Sponsoring Agency Code	
15. Supplementary Notes This paper is to be presented at the AGARD Specialists Meeting in San Diego, California, on October 6-11, 1991.					
16. Abstract The CAP-TSD (Computational Aeroelasticity Program - Transonic Small Disturbance) code, developed at the NASA Langley Research Center, is applied to the Active Flexible Wing (AFW) wind-tunnel model for prediction of the model's transonic aeroelastic behavior. A semi-span computational model is used for evaluation of symmetric motions and a full-span model is used for evaluation of antisymmetric motions. Static aeroelastic solutions using CAP-TSD are computed. Dynamic (flutter) analyses are then performed as perturbations about the static aeroelastic deformations and presented as flutter boundaries in terms of Mach number and dynamic pressure. Flutter boundaries that take into account modal refinements, vorticity and entropy corrections, antisymmetric motions and sensitivity to the modeling of the wing tip ballast stores are also presented and compared with experimental flutter results.					
17. Key Words (Suggested by Author(s)) Transonic Aeroelasticity CAP-TSD Active Flexible Wing Flutter				18. Distribution Statement Unclassified - Unlimited Subject Category 02	
19. Security Classif. (of this report) Unclassified		20. Security Classif. (of this page) Unclassified		21. No. of pages 12	
				22. Price A03	